Observations and Calculations of Light Scattering from Clusters of Spheres

Stephen Holler, Jean-Claude Auger, Brian Stout, Yongle Pan, Jerold R. Bottiger, Richard K. Chang, and Gorden Videen

Army Research Laboratory

Adelphi, MD 20783-1197

Observations and Calculations of Light Scattering from Clusters of Spheres

Stephen Holler
Yale University

Jean-Claude Auger, Brian Stout
Université Pierre et Marie Curie

Yongle Pan
New Mexico State University

Jerold R. Bottiger
U.S. Army Edgewood Chemical Biological Center

Richard K. Chang
Yale University

Gorden Videen
Information Science and Technology Directorate, ARL

Abstract

Two-dimensional angular optical scattering (TAOS) from clusters of polystyrene latex spheres is measured in the near-forward and near-backward directions. In both cases, the scattering pattern contains a rich and complicated structure due to the interaction and interference of the light among the primary particles. Calculations are made for aggregates similar to those generated experimentally that demonstrate the rich structure in the scattering pattern. A comparison of the experimental and theoretical TAOS gives good qualitative agreement.

Contents

Figures

Tables

1. Introduction

Recently there has been experimental [1–3] and theoretical [2,4–7] interest in the optical properties of airborne microparticle aggregates. Such aerosols have been found to play important roles in myriad fields, including industrial, environmental, and health sciences [8], atmospheric remote sensing [9], and astrophysical studies of scattering by planetary [10] and interstellar [11] dust particles. This interest is primarily piqued by the many and/or potentially harmful materials that form clusters of smaller primary particles. For example, carbon (soot) particles, which play an important role in the heat balance of the earth, are often found in fractal aggregates [12]. While the primary particles may be in the Rayleigh regime, the overall cluster is not, so it exhibits fundamentally different optical properties. Other systems of interest include dense clusters of spores that can pose a threat as a biological warfare agent [13]. One possible means for determining shape and structure information about airborne microparticles is to investigate their angular light scattering. Often this is done in only one angular dimension (θ). However, a growing number of researchers are presenting the angular intensity distribution of the scattered light as a function of two angles (θ, ϕ) [3,7,14–17]. Since the angular intensity distribution of nonspherical particles (e.g., microparticle aggregates, oblate and prolate spheroids, etc) has an azimuthal (ϕ) as well as polar (θ) dependence, observation of the two-dimensional angular optical scattering (TAOS) is useful for determining shape and structure information about such nonspherical particles.

In this report, we compare theoretical calculations and experimental results of the TAOS from a three-dimensional, close-packed cluster of spherical primary particles. First, in section 2, we discuss the theoretical technique for calculating the light scattering from an aggregate. Section 3 highlights the experimental arrangement and discusses the generation of the clusters. We present the experimental and theoretical results in section 4. In section 5 we summarize our work and present ideas for future investigations. Finally, the appendices outline the translation addition theorem for spherical wave functions and discuss some relevant aspects for the computational work.

2. Theory

In this section, we develop a model that can be used to calculate the differential scattering cross section of an aggregate composed of many dielectric spheres. Mie introduced the exact solution for the scattering of a plane electromagnetic wave by a single isotropic homogeneous sphere in 1908 [18]. The vector wave equation can be derived by different approaches, such as Hertz vectors [19], the separation of variable solutions (via the scalar wave equation) [20], or T-matrix formalism, introduced by Waterman [21]. We have chosen this last approach because it can be extended to derive the theoretical solution of the multiple scattering of light by an aggregate of spheres. The model includes the multiple scattering that occurs between the spheres, and the formulation is developed to optimize calculations.

2.1 The Vector Wave Equation

In a spherical coordinate system, the linear-independent solution of the vector wave equation (Helmholtz equation) in a source-free, homogeneous medium is the independent, divergenceless vector spherical wave functions $\Psi_{\sigma mn}(kr, \theta, \phi)$:

$$\Re e \Psi_{1mn}(kr, \theta, \phi) = \sqrt{\gamma_{mn}} \left\{ \left[\frac{im}{\sin\theta} j_n(kr) \right] P_n^m(\cos\theta) \exp(im\phi) \widehat{\theta} \right. \tag{1}$$
$$\left. - j_n(kr) \frac{\partial}{\partial\theta} P_n^m(\cos\theta) \exp(im\phi) \widehat{\phi} \right\},$$

$$\Re e \Psi_{2mn}(kr, \theta, \phi) = \sqrt{\gamma_{mn}} \left\{ \frac{n(n+1)}{kr} j_n(kr) P_n^m(\cos\theta) \exp(im\phi) \widehat{r} \right. \tag{2}$$
$$+ \left[\frac{1}{kr} \frac{\partial}{\partial r} r j_n(kr) \right] \frac{\partial}{\partial\theta} P_n^m(\cos\theta) \exp(im\phi) \widehat{\theta}$$
$$\left. + \left[\frac{im}{kr \sin\theta} \frac{\partial}{\partial r} r j_n(kr) \right] P_n^m(\cos\theta) \exp(im\phi) \widehat{\phi} \right\},$$

where $j_n(kr)$ is the set of spherical Bessel functions of the first kind having complex argument kr; $k = \frac{2\pi}{\lambda}$ is the propagation constant for the medium; and $P_n^m(\cos\theta)$ are the associated Legendre functions of the first kind and of degree n and order m, where n and m are integers defined on the intervals

$1 \leq n \leq \infty$ and $-n \leq m \leq n$. The time-harmonic convention is $\exp(-i\omega t)$. The factor $\gamma_{mn} = \frac{(2n+1)(n-m)!}{4\pi n(n+1)(n+m)!}$ serves to normalize the spherical wave functions with the angular variables θ and ϕ. At large r, the scattered fields can be expressed with the vectors $\Psi_{imn}(kr, \theta, \phi)$ that are obtained by replacement of the Bessel functions $j_n(kr)$ with the Hankel functions of the first kind $h_n^{(1)}(kr) = j_n(kr) + iy_n(kr)$. Then, $\Re e$ stands for "the regular part of."

Consider a medium of real refractive index n_0, where a plane electromagnetic wave characterized by a propagation constant k_0 and wavelength λ_0 impinges on a dielectric sphere of complex refractive index n_1 and propagation constant k_1. According to the Mie theory, the incident field ($\mathbf{E}_{\text{inc}}, \mathbf{H}_{\text{inc}}$) and the scattered field ($\mathbf{E}_{\text{sca}}, \mathbf{H}_{\text{sca}}$) can be expanded in terms of infinite series of spherical vector wave functions:

$$\mathbf{E}_{\text{inc}} = \sum_{n=1}^{n=\infty} \sum_{m=-n}^{m=n} [a_{1mn}\Re e\Psi_{1mn} + a_{2mn}\Re e\Psi_{2mn}] = \sum_{\sigma,m,n} a_{\sigma mn}\Re e\Psi_{\sigma mn}, \quad (3)$$

$$\mathbf{H}_{\text{inc}} = \frac{1}{i\eta_\circ} \sum_{n=1}^{n=\infty} \sum_{m=-n}^{m=n} [a_{2mn}\Re e\Psi_{1mn} + a_{1mn}\Re e\Psi_{2mn}]$$

and

$$\mathbf{E}_{\text{sca}} = \sum_{n=1}^{n=\infty} \sum_{m=-n}^{m=n} [f_{1mn}\Psi_{1mn} + f_{2mn}\Psi_{2mn}] = \sum_{\sigma,m,n} f_{\sigma mn}\Re e\Psi_{\sigma mn}, \quad (4)$$

$$\mathbf{H}_{\text{sca}} = \frac{1}{i\eta_\circ} \sum_{n=1}^{n=\infty} \sum_{m=-n}^{m=n} [f_{2mn}\Psi_{1mn} + f_{1mn}\Psi_{2mn}],$$

where $\eta_\circ = \frac{\omega\mu}{k_\circ}$.

2.2 T-Matrix for a Single Dielectric Sphere

The T-matrix introduced by Waterman [21] ($\overline{\mathbf{T}}$) converts the expansion coefficients of the incident wave ($a_{\sigma mn}$) impinging on an arbitrarily shaped particle to the expansion coefficients of the radiated scattering wave ($f_{\sigma mn}$) through the relation

$$\mathbf{f} = \overline{\mathbf{T}}\mathbf{a}. \quad (5)$$

The elements of the T-matrix are independent of the incident and scattered fields. They depend only on the intrinsic features of the scattering particle (shape, size parameter, and complex refractive index) and on its orientation with respect to the coordinate system. For a spherical particle, the elements

3

of the T-matrix are greatly simplified, and it is now well known that application of the boundary condition on the spherical interface yields

$$T_{1mn,1m'n'} = -\delta_{mm'}\delta_{nn'} \frac{j_n(k_1r_0)[k_0r_0 j_n(k_0r_0)]' - j_n(k_0r_0)[k_1r_0 j_n(k_1r_0)]'}{j_n(k_1r_0)[k_0r_0 h_n(k_0r_0)]' - h_n(k_0r_0)[k_1r_0 j_n(k_1r_0)]'} \,, \tag{6}$$

$$T_{2mn,2m'n'} = -\delta_{mm'}\delta_{nn'} \frac{\frac{k_1^2}{k_0^2} j_n(k_1r_0)[k_0r_0 j_n(k_0r_0)]' - j_n(k_0r_0)[k_1r_0 j_n(k_1r_0)]'}{\frac{k_1^2}{k_0^2} j_n(k_1r_0)[k_0r_0 h_n(k_0r_0)]' - h_n(k_0r_0)[k_1r_0 j_n(k_1r_0)]'} \,, \tag{7}$$

$$T_{1mn,2m'n'} = T_{2mn,1m'n'} = 0 \,, \tag{8}$$

where the primes denote derivatives with respect to the arguments of the Bessel functions.

2.3 Expansion of the Incident Plane Wave

The incident plane wave can be expanded in terms of vector spherical wave functions for both polarization states, TE and TM (transverse electric and transverse magnetic, respectively):

$$a_{1mn}^{\text{TM}} = \sqrt{\zeta_{mn}} \, i^{n+3} \frac{m}{\sin\theta_i} P_n^m(\cos\theta_i) \exp(-im\phi_i) \,, \tag{9}$$

$$a_{2mn}^{\text{TM}} = \sqrt{\zeta_{mn}} \, i^{n+3} \frac{d}{d\theta} P_n^m(\cos\theta_i) \exp(-im\phi_i) \,, \tag{10}$$

$$a_{1mn}^{\text{TE}} = \sqrt{\zeta_{mn}} \, i^{n+2} \frac{d}{d\theta} P_n^m(\cos\theta_i) \exp(-im\phi_i) \,, \tag{11}$$

$$a_{2mn}^{\text{TE}} = \sqrt{\zeta_{mn}} \, i^{n+2} \frac{m}{\sin\theta_i} P_n^m(\cos\theta_i) \exp(-im\phi_i) \,, \tag{12}$$

where the factor $\zeta_{mn} = \frac{4\pi(2n+1)(n-m)!}{n(n+1)(n+m)!}$ is introduced for consistency with the normalization chosen for relations (1) and (2).

2.4 Basis of the Analytical Problem

Consider a cluster of N isotropic, homogeneous, compact, randomly dispersed spheres with radii a_i and complex refractive indices n_s^i. The center of each sphere O_i is defined in a principal coordinate system $\mathbf{R}_0$ by a position vector $\mathbf{r}_i$. The relative position vector between two arbitrary spheres i and j is defined by $\mathbf{r}_{ij}$. Applying the superposition principle of electromagnetic theory, we find that the total external field $\mathbf{E}_{\text{tot}}$ is the summation of the incident wave from the original source $\mathbf{E}_{\text{inc}}$, with all the scattered fields $\mathbf{E}_{\text{sca}}^i$:

$$\mathbf{E}_{\text{tot}} = \Re e \mathbf{\Psi}(k_0 |\mathbf{r} - \mathbf{r}_0|)\mathbf{a}^0 + \sum_{i=1}^{N} \mathbf{\Psi}(k_0 |\mathbf{r} - \mathbf{r}_i|)\mathbf{f}^{i(N)}. \tag{13}$$

4

Solving the total electric field scattered by an aggregate of spheres amounts to evaluating the scattered field by each individual sphere in the cluster. It is then necessary to translate the entire scattered field on a common basis to get an exact single analytical expression of the total field scattered by the aggregate.

2.5 Solving the Multiple Scattering Equation

In multiple-scattering theory, the field incident upon the ith scatterer is due to the contribution of the field from the original source $\mathbf{E}_{inc}$ and the scattered fields $\mathbf{E}_{sca}^j$ from the other j particles in the cluster. This field, called the "excitation field" $\mathbf{E}_{exc}^i$, has the formulation

$$\mathbf{E}_{exc}^i = \mathbf{E}_0 + \sum_{\substack{j=1 \\ j \neq i}}^{N} \mathbf{E}_{sca}^j. \tag{14}$$

The T-matrix formulation (eq (5)) leads to the relation $\mathbf{E}_{sca}^i = \bar{\mathbf{T}}^{i(1)} \mathbf{E}_{exc}^i$, where $\bar{\mathbf{T}}^{i(1)}$ is the isolated-scatterer T-matrix for the ith scatterer. Then, using the expansion in terms of spherical vector wave functions of each field, we have

$$\mathbf{E}_{sca}^i = \bar{\mathbf{T}}^{i(1)}[\Re e \vec{\Psi}(k_0\,|r - r_0|)\mathbf{a}^0 + \sum_{\substack{j=1 \\ j \neq i}}^{N} \Psi(k_0\,|r - r_i|)f^{j(N)}]. \tag{15}$$

In the above expression (eq (15)), the incident field is expanded in the principal coordinate system $R_0(kr_0, \theta_0, \phi_0)$, whereas the scattered fields from each sphere are expressed in the coordinate systems of the scatterers $R_j(kr_j, \theta_j, \phi_j)$. To solve the multiple scattering problems, it is necessary to express both terms in the ith scatterer coordinate system. Applying the translational addition theorem for the spherical vector wave functions (eq (A-1) and (A-2) in app A), and using the expansion coefficient representation of each field, we get from equation (15)

$$f^{j(N)} = \bar{\mathbf{T}}^{i(1)}\left(\bar{\beta}(i, 0)\mathbf{a}^0 + \sum_{\substack{j=1 \\ j \neq i}}^{N} \bar{\alpha}(i, j)f^{j(N)} \right), \quad i = 1, ..., N, \tag{16}$$

where $\bar{\beta}(i, 0)$ and $\bar{\alpha}(i, j)$ are the translation matrices for the incident and scattered fields, respectively. This last relation defines a group of N-coupled linear equations whose unknown variables are the expansion coefficients of the scattered field of each individual sphere. The solution can

be found with different techniques, such as the order of scattering [4], the direct inversion matrix [22], or the iteration method [23]. Nevertheless, it is convenient to introduce $\bar{\mathbf{T}}^{i(N)}$, the N-scatterer T-matrix of the ith scatterer. This formulation includes all the information about multiple scattering effects due to the presence of the N scatterers. It directly links the incident field E_0 to the scattered field of the ith scatterer by the relation

$$\mathbf{f}^{i(N)} = \bar{\mathbf{T}}^{i(N)}\mathbf{a}^i = \bar{\mathbf{T}}^{i(N)}\bar{\beta}(i,0)\mathbf{a}^0. \tag{17}$$

As $\mathbf{f}^{i(N)}$ is defined in the coordinate system of the ith scatterer, $\mathbf{a}^i$ is also. Then, from equation (13) and by application of the translational addition theorem (eq (A-3)) once more, the total scattered field coefficients in the principal coordinate system have the form

$$\mathbf{f}^{\mathrm{T}(N)} = \sum_{i=1}^{N} \bar{\beta}(0,i)\bar{\mathbf{T}}^{i(N)}\bar{\beta}(i,0)\mathbf{a}^0. \tag{18}$$

It is possible to introduce the global T-matrix of the cluster $\bar{\mathbf{T}}^{\mathrm{T}(N)}$, which directly converts the incident field coefficients to the total scattered field coefficients:

$$\mathbf{f}^{\mathrm{T}(N)} = \bar{\mathbf{T}}^{\mathrm{T}(N)}\mathbf{a}^0 , \tag{19}$$

with

$$\bar{\mathbf{T}}^{\mathrm{T}(N)} = \sum_{i=1}^{N} \bar{\beta}(0,i)\bar{\mathbf{T}}^{i(N)}\bar{\beta}(i,0). \tag{20}$$

The global T-matrix is independent of the incident field and only depends on cluster configuration; therefore, it can be used in computations for any direction and polarization state of the incident wave. It is also very useful for computing orientationally averaged light scattering through the use of the rotational addition theorem.

Substitution of equation (17) into equation (16) results in a new linear matrix equation, in which the unknown variables are the N-scatterer T-matrices of each sphere. This system can be solved with an iterative or a recursive algorithm [5,24]. However, for certain dense aggregates, the iterative algorithm cannot converge, because the method assumes the primary contribution is the incident field. For this reason, we use the recursive T-matrix

algorithm (RTMA) developed by Chew as the basis of our work. The results can be expressed by these two equations [24]:

$$\bar{\mathbf{T}}^{N+1(N+1)}\bar{\beta}(N+1,0) = \left[\bar{\mathbf{I}} - \bar{\mathbf{T}}^{N+1(1)}\sum_{i=1}^{n}\bar{\alpha}(N+1,i)\bar{\mathbf{T}}^{i(N)}\bar{\beta}(i,0)\bar{\alpha}(0,N+1)\right]^{-1}$$

$$\times \bar{\mathbf{T}}^{N+1(1)}\left[\bar{\beta}(N+1,0) + \sum_{i=1}^{n}\bar{\alpha}(N+1,i)\bar{\mathbf{T}}^{i(N)}\bar{\beta}(i,0)\right], \qquad (21)$$

$$\bar{\mathbf{T}}^{i(N+1)}\bar{\beta}(i,0) = \bar{\mathbf{T}}^{i(N)}\bar{\beta}(i,0)\left[\bar{\mathbf{I}} + \bar{\alpha}(0,N+1)\bar{\mathbf{T}}^{N+1(N+1)}\bar{\beta}(N+1,0)\right], \ i \leq N. \qquad (22)$$

The effect of the $(N+1)$ sphere in the aggregate acts as a perturbation for the whole system. Then, the individual multiple-scattering T-matrices $\bar{\mathbf{T}}^{i(N+1)}$ of the $(N+1)$-sphere cluster are evaluated from the individual multiple-scattering T-matrices $\bar{\mathbf{T}}^{i(N)}$ of the N-sphere cluster.

3. Experiment

The experimental setup, shown in figure 1, consists of a particle generator, used to create the clusters, and an apparatus to illuminate the clusters and measure their two-dimensional angular scattering pattern. Clusters of polystyrene latex (psl) spheres are generated with an ink-jet aerosol generator (IJAG) [25] from a solution of psl spheres and water, loaded into an empty ink-jet cartridge (Hewlett Packard 51612A "BlankJet"), which is mounted on the IJAG's drying column. The IJAG controller box sequentially triggers (either from 1 Hz to 2 kHz or singly, on demand) each of the 12 nozzles in the cartridge to produce water droplets (50 μm diameter) containing psl sphere inclusions. The number of primary particles within the water droplet follows Poisson statistics and depends on the concentration of the slurry within the cartridge. By varying the concentration, we can generate clusters of different sizes. After being ejected from the ink-jet cartridge, the droplets are often accompanied by small satellite droplets. These secondary droplets are removed with a winnow flow, while the large primary droplet is entrained within an airflow that carries it through the drying column. The drying column is heated to $\sim$105 °C, so that as the wet droplets with inclusions traverse the column, the water evaporates, leaving a dry aggregate of primary particles. At the end of the column is a tapered nozzle with an exit port of 1 mm. The clusters emerge from the nozzle and fall into the scattering volume of the measuring apparatus.
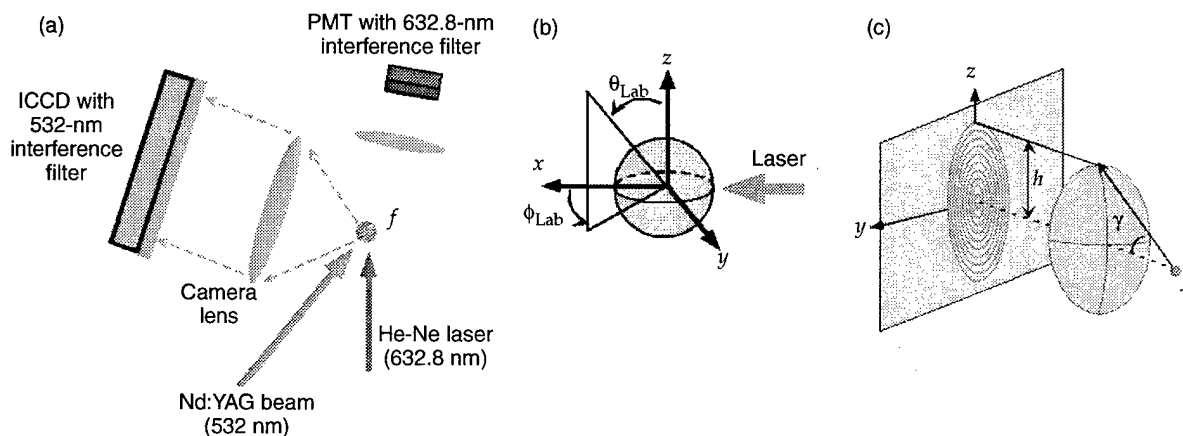

Figure 1. TAOS measurements: (a) experimental setup, (b) laboratory coordinate system, and (c) illustration of Abbé sine condition.

Although the IJAG may fire periodically, the changing droplet size and the irregular shape of the aggregates prevents the clusters from emerging in a periodic fashion. Due to the asynchronous passage of particles through the scattering volume, it is necessary to detect when a cluster is in the correct location. The presence of a falling cluster is detected by a continuous-wave He-Ne trigger laser (632.8 nm) and a photomultiplier tube (PMT) with a narrow bandpass filter. As the aggregate enters the scattering volume, it crosses the He-Ne trigger beam and scatters light toward the PMT. Detection of a signal with the PMT initiates the trigger sequence for the TAOS measurement.

Upon the laser receiving a trigger pulse, the second harmonic ($\lambda = 532$ nm) of a Q-switched (30-ns pulse) Nd:YAG illuminates the falling cluster. The elastic scattered light is then collected in either the near-forward or near-backward regions with an f/number = 1.2 camera lens used in the Abbé sine condition [26]. Under this condition, the lens is positioned so that the falling particle is in the back focal plane of the lens. Rays of light that scatter off the particle and enter the lens at an angle γ emerge parallel with a displacement h, given by

$$h = f \sin \gamma, \tag{23}$$

where f is the focal length of the lens. The emerging parallel light is then recorded with an intensified charge-coupled device (ICCD) camera with a narrow bandpass filter, so that only the scattered 532-nm light is recorded.

For our experiments, the coordinate system of the laboratory is taken such that the clusters fall in the $-z$ direction and the laser propagates parallel to the x-axis (see fig. 1(b)). The Abbé sine condition then relates the y-z coordinate of the ICCD camera to the θ_{Lab}-ϕ_{Lab} scattering angles in the laboratory frame. The geometry of the sine condition is shown in figure 1(c). This choice of coordinate system is nonstandard in the performance of TAOS calculations. Typically, and as is done for our calculations, the laser propagates along the z-axis. In that case, the aggregates would be falling in the $-x$ direction. The correspondence between the calculation and laboratory frames is such that $(x, y, z)_{\mathrm{Calc}} \longleftrightarrow (z, -y, x)_{\mathrm{Lab}}$. In order to make comparisons between experimental results and theoretical calculations, it is useful to transform the calculations into the laboratory-frame coordinate system. This is done by comparison of the two coordinate systems and use of the sine condition of equation (23). The resulting transformation is

$$\theta_{\mathrm{Lab}} = \cos^{-1}\left(\sin \theta_{\mathrm{Calc}} \cos \phi_{\mathrm{Calc}}\right), \tag{24}$$
$$\phi_{\mathrm{Lab}} = \phi_0 + (-1)^j \sin^{-1}\left(-\sin \theta_{\mathrm{Calc}} \sin \phi_{\mathrm{Calc}}\right),$$

where θ_{Lab} and ϕ_{Lab} are the scattering angles in the laboratory coordinate frame, θ_{Calc} and ϕ_{Calc} are the scattering angles in the calculation frame, and ϕ_0 is either 0° with $j = 0$ for forward scattering or 180° with $j = 1$ for backward scattering.

9

4. Results and Discussion

To ensure the proper operation of our apparatus, TAOS measurements were performed on single psl spheres of two different sizes. Dilute solutions of 22- and 2.29-μm-diameter psl spheres were prepared and loaded into ink-jet cartridges. The TAOS measurements for both sizes were consistent with Mie theory, demonstrating the ring structure associated with light scattering from a sphere. With this verification, we could confidently perform TAOS measurements on aggregates of the 2.29-μm-diameter psl spheres.

Aggregates of 2.29-μm-diameter psl spheres (refractive index $n = 1.59$) are created with the IJAG. The slurry is mixed at 0.7 mg of spheres per ml of water. In addition, a small amount (0.01%) of surfactant (Tween-20) is added to the water to help the mixture's flow properties (necessary for passage inside the narrow channels of the cartridge). The clusters are characterized by an aerodynamic particle sizer (APS), scanning electron microscopy (SEM), and optical microscopy. We determine the average number of spheres per cluster by turning off the oven heater and allowing it to cool. Wet droplets containing psl spheres are allowed to fall through the column and splatter onto a microscope slide. The water in each splat evaporates, leaving a monolayer of particles that we count with an optical microscope to determine the average number of primary particles per cluster.

The uniformity of the droplets can be inferred from a count of the number of primary particles included in a sampling of droplets. In figure 2 we show the results of counting the number of 2.29-μm psl spheres (N_{sph}) in each of 227 randomly selected splats of wet droplets. The fraction of the 227 clusters containing N_{sph} spheres is plotted versus N_{sph}. The most probable number of spheres was found to be 18. Also plotted is the Poisson distribution probability for finding N_{sph} spheres in a cluster, given that the average N_{sph} is 18. The two sets of data are in good agreement, as one would expect if the original droplets were monodisperse. The data points indicating more than about 40 spheres in a cluster are probably where two or three droplets hit the microscope slide at the same location. Geometric sizing with a scanning electron microscope found this cluster sample to have a mean geometric diameter of 6.7 μm. Figure 3(a) shows an SEM micrograph of a typical psl cluster.

Calculations are performed for a close-packed cluster containing primary particles of the same size parameter ($x_{\mathrm{p.p.}} = \frac{2\pi a}{\lambda} \approx 13.3$) as those used in the

Figure 2. Fraction of 227
clusters containing N_{sph}
spheres plotted versus
N_{sph}. Solid curve repre-
sents Poisson distribution
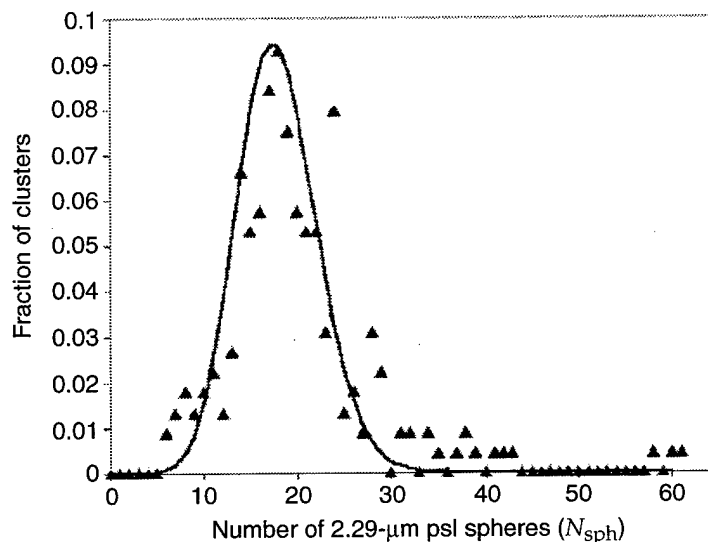given that most probable
number of spheres is 18.

Figure 3. Comparison of
(a) SEM of typical cluster
for which TAOS meas-
urements were performed;
(b) Mathematica default
representation of cluster
used in numerical calcu-
lations (primary particle
coordinates are given in
table 1); (c) representation
of unrotated ($\tau = 0°$)
theoretical cluster viewed
along z-axis of calculation
frame (i.e., cluster as seen
from incident plane wave);
and (d) realization of
theoretical cluster rotated
by 45° and viewed along
z-axis of calculation frame.
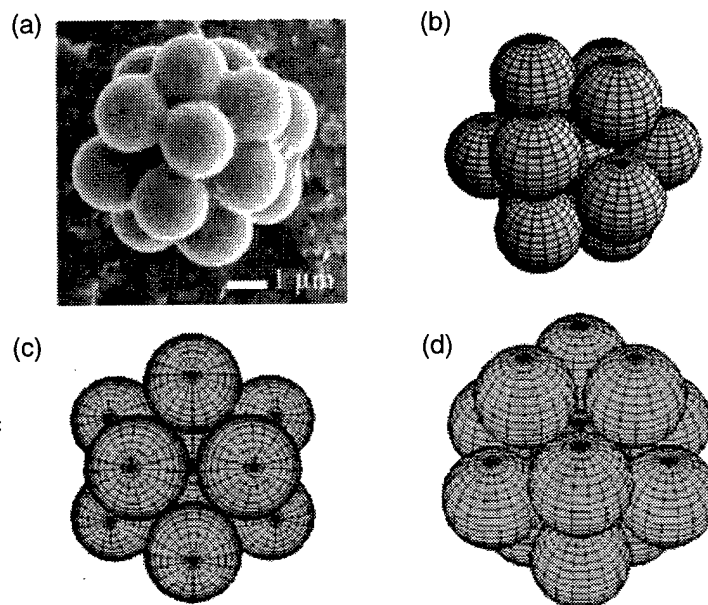
experiment. For the aggregate size parameter to be comparable to the mean
experimental size parameter ($x_{clus.} \approx 40$), 13 spheres are arranged as shown
in figure 3(b). The coordinates of each of the primary particles are given
in table 1. Since falling clusters in the experiment are randomly oriented,
the calculations are performed at different tilt angles (τ) so a reasonable
comparison can be made. Figure 3(b) represents the Mathematica default
view of the theoretically generated cluster. The view along the calculation

11

Table 1. Coordinates of spheres used for cluster calculation.

Sphere	x	y	z
1	0.000	0.000	0.000
2	1.925	−1.189	0.000
3	0.000	1.925	−1.189
4	−1.189	0.000	1.925
5	0.000	−1.925	−1.189
6	1.189	0.000	1.925
7	−1.925	1.189	0.000
8	1.189	0.000	−1.925
9	−1.925	−1.189	0.000
10	1.925	1.189	0.000
11	0.000	−1.925	1.189
12	−1.189	0.000	−1.925
13	0.000	1.925	1.189

z-axis (i.e., the view of the cluster seen from the illuminating laser) for the unrotated cluster ($\tau = 0°$) is shown in figure 3(c). Rotation of the cluster through $\tau = 5°$ yields a slightly different view from that seen in figure 3(c) and is not shown. The cluster rotated by $\tau = 45°$ and viewed from the illuminating laser is shown in figure 3(d). The cluster seen in this orientation is remarkably similar to that shown in the SEM micrograph of figure 3(a).

The random orientation of the aggregates emerging from the IJAG makes it impossible to know for which angles to calculate the TAOS. Because of this uncertainty, we chose to look at three different orientations ($\tau = 0°, 5°$, and $45°$). To get a sense of what the numerical calculations of the TAOS look like in the laboratory coordinate frame, we used equation (24) to transform the calculations. The resulting transformed forward and backward TAOS calculations for the three different orientations considered are shown in figure 4. Due to the high-intensity forward-scattering peak, the forward-scattering calculations are plotted on a log scale. Also shown are the regions observed experimentally. In the forward direction, the TAOS measurements are made for $16° \leq \theta_{Calc} \leq 44°$, while the near-backward observations are made for $120° \leq \theta_{Calc} \leq 148°$. These angular regions correspond to the area bound by the white circles. The actual angular coverage of the detector is denoted by the white rectangle.

As previously stated, the random orientation of the clusters emerging from the IJAG makes it impossible to know the angles for which calculations should be performed. Our comparisons are limited to three different tilt angles that allow us to view the cluster in three representative orientations: one of high symmetry, one with slightly less symmetry, and one

12

Figure 4. Forward and backward TAOS calculations transformed into laboratory coordinate frame for three different cluster orientations: (a) 0°, (b) 5°, and (c) 45°.
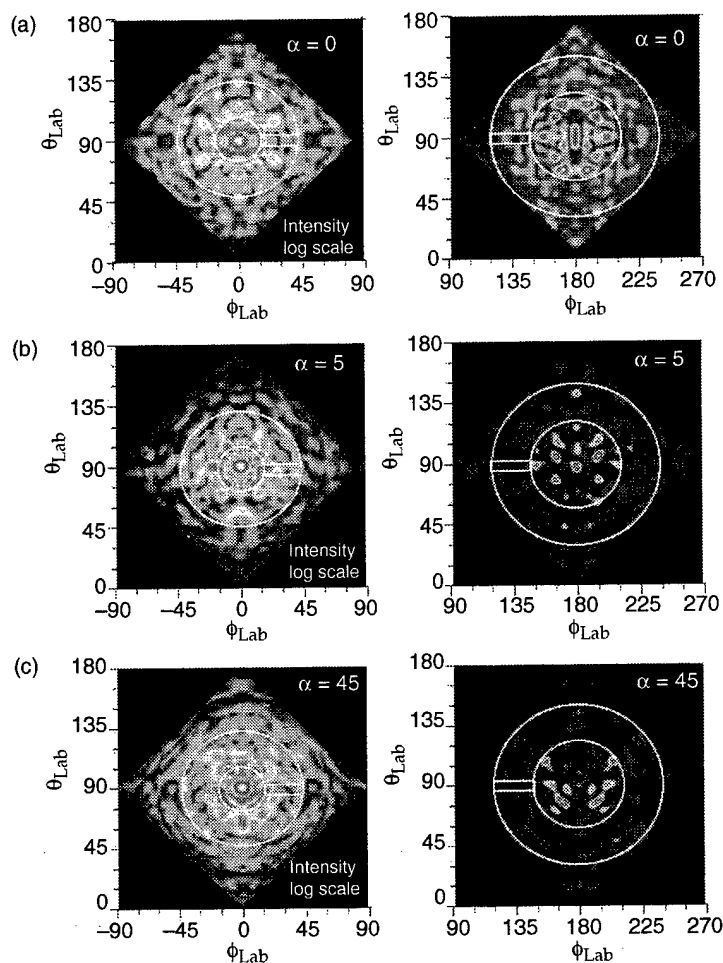
whose symmetry has been broken. However, the falling aggregates are also free to rotate in the ϕ_{Calc} direction. Rather than calculate at a number of different (θ_{Calc}, ϕ_{Calc}) orientations, we chose to simply compare experiment and theory by fixing the tilt angle (τ) and scanning through ϕ_{Calc} within the bound regions of figure 4. By sweeping the white rectangle in figure 4 through the bound region, we could choose a portion of the calculated TAOS pattern to compare with the experimental results. Comparisons were made at various values of ϕ_{Calc} until reasonable correspondence was found. This method for comparing our results is supported by calculations of light scattering by the theoretical cluster (fig. 3) for parallel and perpendicular polarizations. These calculations, which are equivalent to keeping the polarization fixed and rotating the cluster through 90°, show little difference in the TAOS pattern, and thus give us confidence that our comparison method is reasonable.

Figure 5 shows eight representative TAOS measurements made in the near-forward region ($16° \leq \phi_{Lab} \leq 44°$, $87° \leq \theta_{Lab} \leq 94°$). They demonstrate the rich speckle pattern that arises from near-field interactions and multiple scattering events among the primary particles. Figure 6 shows eight calculated TAOS patterns that qualitatively resemble the experimental data of figure 5. These eight plots are representations of different ϕ_{Calc} locations of the data within the bound regions of figure 4 ($16° \leq \theta_{Calc} \leq 44°$), presented

Figure 5. Eight representative TAOS measurements in near-forward scattering direction.
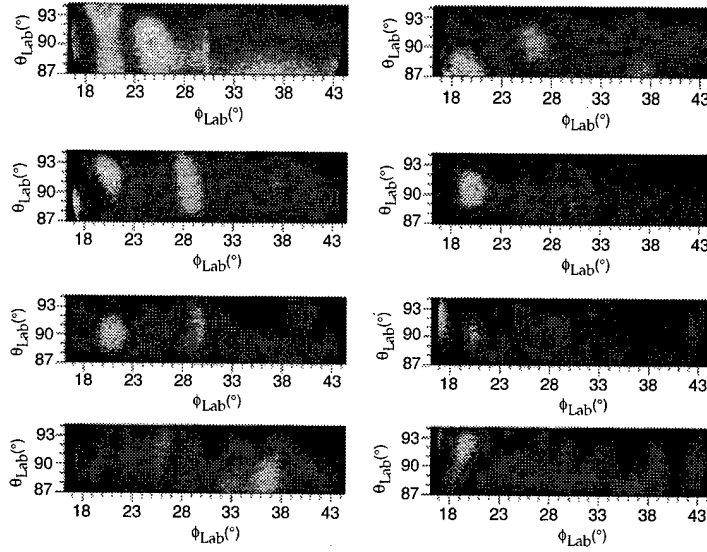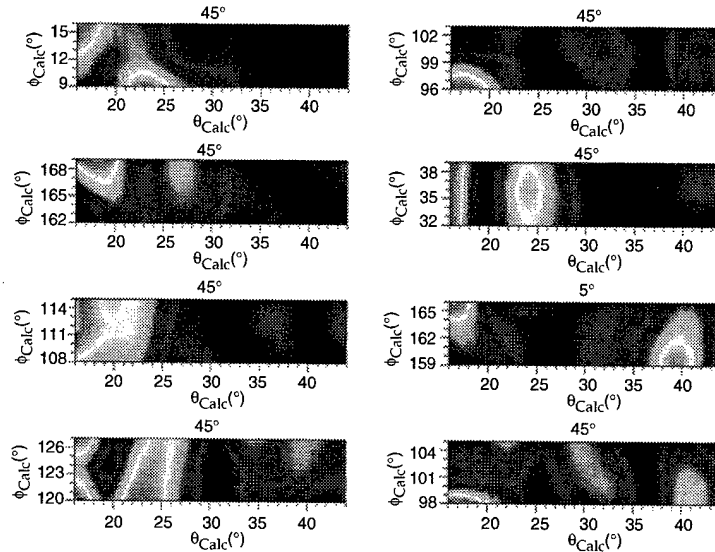

Figure 6. Near-forward TAOS calculations showing qualitative features found in experiments.

14

in a format such that the angular coverage within each plot corresponds to the same area as the ICCD camera. The best correspondence is found for the cluster tilted by 45°. This is due to the lack of symmetry for this cluster orientation. For the unrotated cluster, there exists a large amount of symmetry, since the primary particles are arranged in an almost crystalline fashion. Tilting the cluster by 5° does little to remove the symmetry of the aggregate; however, some correspondence with the experiment is found.

For the near-backward region ($120° \leq \phi_{Lab} \leq 148°$, $87° \leq \theta_{Lab} \leq 94°$), eight representative TAOS measurements are shown in figure 7. They, too, show the rich speckle pattern; however, the intensity patches seem to exhibit a more random orientation. The same type of comparison between experiment and calculation is presented for the backward-scattering case. Figure 8 shows the results of this comparison with eight numerical calculations for the TAOS in the bound angular region in figure 4 ($120° \leq \theta_{Calc} \leq 148°$). A greater correspondence between experiment and theory is found for the cluster tilted by 45°; however, in spite of the high symmetry, correspondence is also seen for the unrotated and 5° tilted cluster orientations.

Although the comparisons presented in figures 5 through 8 are not quantitative, they do show some common features persistent in both the experimental and theoretical results. Most notably, the comparison shows a correspondence in the frequency of the speckle features, as well as relatively good agreement in the size of the peaks. Previously reported TAOS measurements on larger ($\sim$11 μm) clusters of the 2.29-μm-diameter psl spheres demonstrate a higher frequency speckle pattern with

Figure 7. Eight representative TAOS measurements in near-backward scattering direction.
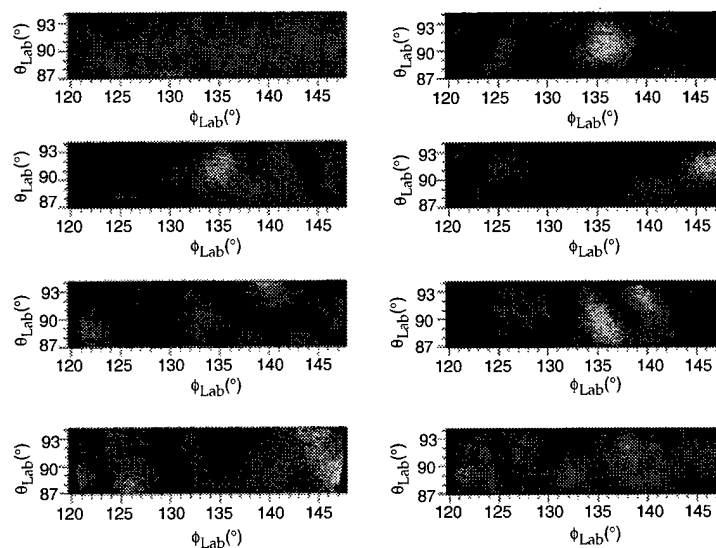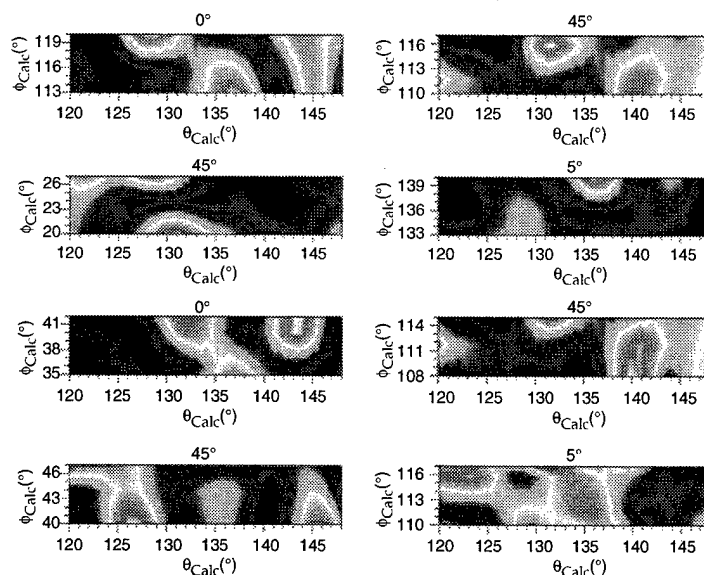

15

Figure 8. Near-backward TAOS calculations showing qualitative features found in experiments.

a corresponding decrease in the peak size [3]. Quantitative comparisons between experiment and theory are not possible because of the limited information regarding cluster configuration and orientation at the time of the measurement. Despite the inability to make a quantitative comparison, there are some features present in all the calculations that are observed in the experiment. It is these features that should make it possible to determine the primary particle size, as well as overall cluster size. What is needed to better predict the TAOS is knowledge of the cluster orientation and a more detailed understanding of the nature of aggregate formation so that we can more realistically position the primary particles of the cluster used in the calculations. The presence of internal irregularities (e.g., unevaporated liquid within the crystal) can also have a dramatic effect on the TAOS [7].

What we have presented is merely one case demonstrating a qualitative agreement among the features found in the experimentally observed and numerically calculated TAOS patterns for an aggregate of spheres. What happens, then, if the size of the primary particle is changed? The effect of the primary particles on the overall scattering pattern is quite dramatic. The close proximity of the spheres and the corresponding surface roughness of the aggregate lead to near-field effects and multiple scattering events that lead to the breakdown of the smooth, continuous contours associated with scattering from a single sphere. Although we can infer, based on our knowledge of light scattering from a sphere and previous experiments on clusters [3], that as the aggregate size changes the speckle pattern becomes more or less dense, the effect of size changes in the primary particles is less obvious. One might expect that as the primary particle becomes smaller, the island

16

of intensity would become broader; and, in fact, this appears to be the case. Figure 9 shows TAOS calculations of the forward-scattering region in the laboratory frame for two unrotated ($\tau = 0°$) clusters of the same size, but which contain different size primary particles. The effect of primary particle size is noticeable in the forward-scattering region, where diffraction is the dominant component of the scattering. In figure 9(a), the cluster contains 2.0-μm-diameter spheres, while the cluster in figure 9(b) comprises 2.29-μm-diameter spheres. Even for this modest change in diameter, one can clearly see the effect that primary particles have on the angular intensity distribution. The structure of both clusters is the same as that shown in figure 3(c). This symmetry is clearly seen in the diffraction regime of the forward-scattered light. The intensity patches in the TAOS of figure 9(a) are broader, and there appear to be fewer of them. In contrast, the TAOS in figure 9(b) shows sharper peaks, particularly in the diffraction-dominated region, as well as a higher speckle density elsewhere. The TAOS calculations depicted in figure 9 are simply meant to corroborate our results presented above; a more detailed study of the nature of light scattering from clusters with different size primary particles will be published at a later date [27].

Figure 9. Forward TAOS calculations for two clusters of same size comprising primary particles with different sizes: (a) cluster containing 2.0-μm-diameter spheres and (b) cluster containing 2.29-μm-diameter spheres.

17
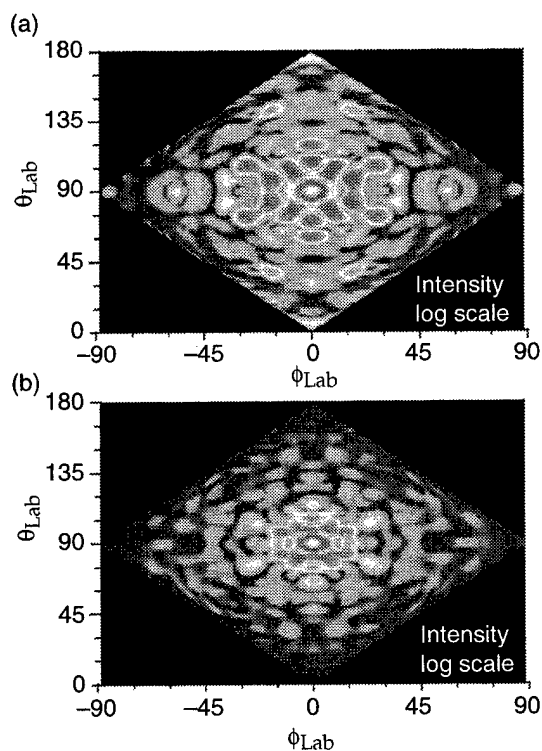
5. Summary

Although the results presented are not yet quantitative, they do offer insight into the nature of light scattering by an aggregate of spherical primary particles. The correspondence between the experimentally observed two-dimensional angular optical scattering and the numerically calculated patterns is good. Both experiment and theory yield the same qualitative features within the same size angular region. The difficulty in making quantitative comparisons lies in unraveling the nature by which aggregates of spheres form and determining a means for discerning the orientation of the falling cluster at the moment of the TAOS measurement. Futhermore, providing for larger angular coverage with the detector would improve the ability to make quantitative comparisons. By far the easiest of these lies in the large format detector, capable of recording the TAOS over a wide angular range.

The complicated morphology of airborne microparticle aggregates makes understanding their light-scattering properties a challenging task. From an experimental viewpoint, it is almost impossible to know the exact structure, orientation, and number of primary particles of the cluster under study. Likewise, memory limits and time constraints often restrict the size of aggregates that can be studied computationally, and the cluster structure is somewhat artificial and "crystalline." Despite these difficulties, experiments and theory are rapidly finding a common ground, and study can only improve in the future.

Acknowledgment

References

1. R. H. Zerull, B.Å.S. Gustafson, K. Schulz, and E. Thiele-Corbach, "Scattering by aggregates with and without an absorbing mantle: Microwave analog experiments," *Appl. Opt.* **32**, 4088–4100 (1993).

2. G. Videen, D. Ngo, and M. B. Hart, "Light scattering from a pair of conducting, osculating spheres," *Opt. Commun.* **125**, 275–287 (1996).

3. S. Holler, Y.-L. Pan, R. K. Chang, J. R. Bottiger, S. C. Hill, and D. B. Hillis, "Two-dimensional angular optical scattering for the characterization of airborne microparticles," *Opt. Lett.* **23**, 1489–1491 (1998).

4. K. A. Fuller, "Scattering and absorption cross sections of compounded spheres. I. Theory for external aggregation," *J. Opt. Soc. Am. A* **11**, 3251–3260 (1994).

5. D. W. Mackowski and M. I. Mishchenko, "Calculation of the T matrix and the scattering matrix for ensembles of spheres," *J. Opt. Soc. Am. A* **13**, 2266–2278 (1996).

6. D. Ngo, G. Videen, and R. Dalling, "Chaotic light scattering from a system of osculating, conducting spheres," *Phys. Lett. A* **227**, 197–202 (1997).

7. G. Videen, W. Sun, and Q. Fu, "Light scattering from irregular tetrahedral aggregates," *Opt. Commun.* **156**, 5–9 (1998).

8. D. R. Bowes, A. M. Langer, and A. N. Rohl, "Nature and range of mineral dusts in the environment," *Phil. Trans. R. Soc. Lond. A* **286**, 593–610 (1977).

9. E. Frejafon, J. Kasparian, P. Rambaldi, B. Vezin, V. Boutou, J. Yu, M. Ulbricht, D. Weidauer, B. Ottobrini, E. de Saeger, B. Krämer, T. Leisner, P. Rairoux, L. Wöste, and J. P. Wolf, "Laser applications for atmospheric pollution monitoring," *Eur. Phys. J. D.* **4**, 231–238 (1998).

10. J. E. Hansen and L. D. Travis, "Light scattering in planetary atmospheres," *Space Sci. Rev.* **16**, 527–610 (1974).

11. D. R. Huffman, "Interstellar grains. The interaction of light with a small particle system," *Adv. Phys.* **26**, 129–230 (1977).

12. C. M. Sorensen, J. Cai, and N. Lu, "Light scattering measurements of monomer size, monomers per aggregate and fractal dimension for soot aggregates in flames," *Appl. Opt.* **31**, 6547–6557 (1992).

13. R. G. Pinnick, S. C. Hill, P. Nachman, G. Videen, G. Chen, and R. K. Chang, "Aerosol fluorescence spectrum analyzer for measurement of single micron-sized airborne biological particles," *Aerosol Sci. Technol.* **28**, 95–104 (1998).

14. P. L. Marston and E. H. Trinh, "Hyperbolic umbilic diffraction catastrophe and rainbow scattering from spheroidal drops," *Science* **312**, 529–531 (1984).

15. P. L. Marston, "Cusp diffraction catastrophe from spheroids: Generalized rainbows and inverse scattering," *Opt. Lett.* **10**, 588–591 (1985).

16. J. P. Barton, "Light scattering calculations for irregularly shaped axisymmetric particles of homogeneous and layered compositions," *Meas. Sci. Technol.* **9**, 151–160 (1998).

17. J. P. Barton, "Electromagnetic field calculations for a sphere illuminated by a higher-order Gaussian beam. II. Far-field scattering," *Appl. Opt.* **37**, 3339–3344 (1998).

18. G. Mie, "Beitrage zur Optik trüber Medien speziell kolloidaler Metallösungen," *Ann. Phys.* **25**, 377–445 (1908).

19. J. Stratton, *Electromagnetic Theory*, McGraw-Hill, New York, 1941.

20. C. F. Bohren and D. R. Huffman, *Absorption and Scattering of Light by Small Particles*, John Wiley & Sons, New York, 1983.

21. P. C. Waterman, "Symmetry, unitarity, and geometry in electromagnetic scattering," *Phys. Rev. D* **3**, 825–839 (1970).

22. A.-K. Hamid, "Electromagnetic scattering by an arbitrary configuration of dielectric spheres," *Can. J. Phys.* **68**, 1419–1428 (1990).

23. Y.-L. Xu, "Electromagnetic scattering by an aggregate of spheres: Far field," *Appl. Opt.* **36**, 9496–9508 (1997).

24. W. C. Chew, *Waves and Field in Inhomogeneous Media*, IEEE Press Series on Electromagnetic Waves, 1990.

25. J. R. Bottiger, P. J. Deluca, E. W. Stuebing, and D. R. VanReenen, "An ink jet aerosol generator," *J. Aerosol Sci.* **29**, suppl. 1, s965–s966 (1998).

26. M. Born and E. Wolf, *Principles of Optics, 6e*, Oxford, Pergamon Press, 1980.

27. J.-C. Auger and G. Videen (in preparation).

Appendix A.   Translation Addition Theorem

Stein[1] and Cruzan[2] first introduced the translation addition theorem of spherical wave functions. This theorem is formed by three different kinds of relations:

$$\Re e\Psi_{1mn}(kr_i,\theta_i,\phi_i) = \sum_{\mu\nu} \Re e A_{\mu\nu}^{mn}(r_{ij},\theta_{ij},\phi_{ij})\Re e\Psi_{1\mu\nu}(kr_j,\theta_j,\phi_j) \qquad (A\text{-}1)$$
$$+ \Re e B_{\mu\nu}^{mn}(r_{ij},\theta_{ij},\phi_{ij})\Re e\Psi_{2\mu\nu}(kr_j,\theta_j,\phi_j) \, ,$$
$$\Re e\Psi_{2mn}(kr_i,\theta_i,\phi_i) = \sum_{\mu\nu} \Re e B_{\mu\nu}^{mn}(r_{ij},\theta_{ij},\phi_{ij})\Re e\Psi_{1\mu\nu}(kr_j,\theta_j,\phi_j)$$
$$+ \Re e A_{\mu\nu}^{mn}(r_{ij},\theta_{ij},\phi_{ij})\Re e\Psi_{2\mu\nu}(kr_j,\theta_j,\phi_j).$$

If $r < r_o$,

$$\Psi_{1mn}(kr_i,\theta_i,\phi_i) = \sum_{\mu\nu} A_{\mu\nu}^{mn}(r_{ij},\theta_{ij},\phi_{ij})\Re e\Psi_{1\mu\nu}(kr_j,\theta_j,\phi_j) \qquad (A\text{-}2)$$
$$+ B_{\mu\nu}^{mn}(r_{ij},\theta_{ij},\phi_{ij})\Re e\Psi_{2\mu\nu}(kr_j,\theta_j,\phi_j) \, ,$$
$$\Psi_{2mn}(kr_i,\theta_i,\phi_i) = \sum_{\mu\nu} B_{\mu\nu}^{mn}(r_{ij},\theta_{ij},\phi_{ij})\Re e\Psi_{1\mu\nu}(kr_j,\theta_j,\phi_j)$$
$$+ A_{\mu\nu}^{mn}(r_{ij},\theta_{ij},\phi_{ij})\Re e\Psi_{2\mu\nu}(kr_j,\theta_j,\phi_j).$$

If $r > r_o$,

$$\Psi_{1mn}(kr_i,\theta_i,\phi_i) = \sum_{\mu\nu} \Re e A_{\mu\nu}^{mn}(r_{ij},\theta_{ij},\phi_{ij})\Psi_{1\mu\nu}(kr_j,\theta_j,\phi_j) \qquad (A\text{-}3)$$
$$+ \Re e B_{\mu\nu}^{mn}(r_{ij},\theta_{ij},\phi_{ij})\Psi_{2\mu\nu}(kr_j,\theta_j,\phi_j) \, ,$$
$$\Psi_{2mn}(kr_i,\theta_i,\phi_i) = \sum_{\mu\nu} \Re e B_{\mu\nu}^{mn}(r_{ij},\theta_{ij},\phi_{ij})\Psi_{1\mu\nu}(kr_j,\theta_j,\phi_j)$$
$$+ \Re e A_{\mu\nu}^{mn}(r_{ij},\theta_{ij},\phi_{ij})\Psi_{2\mu\nu}(kr_j,\theta_j,\phi_j).$$

$A_{\mu\nu}^{mn}$, $\Re e A_{\mu\nu}^{mn}$, $B_{\mu\nu}^{mn}$, and $\Re e B_{\mu\nu}^{mn}$ are translation coefficients that can be expressed in terms of Gaunt coefficients:

$$A_{\mu\nu}^{mn} = \frac{\sqrt{\gamma_{mn}}}{\sqrt{\gamma_{\mu\nu}}} (-1)^{\mu} \sum_{p} a\,(m,\ n|-\mu,\ \nu|p)\,a\,(n,\nu,p) \qquad (A\text{-}4)$$
$$\times\, h_p\,(ka)\,P_p^{m-\mu}\,(\cos\theta_{0k})\,\exp[i\,(m-\mu)\,\phi_{0k}],$$

[1]S. Stein, "Addition theorems for spherical wave function," *Q. Appl. Math.* **19**, 15–24 (1961).

[2]O. R. Cruzan, "Translation addition theorems for spherical vector wave functions," *Q. Appl. Math.* **20**, 33–40 (1962).

$$B_{\mu\nu}^{mn} = \frac{\sqrt{\gamma_{mn}}}{\sqrt{\gamma_{\mu\nu}}} (-1)^{\mu+1} \sum_p a\left(m, n | -\mu, \nu | p, p-1\right) b\left(n, \nu, p\right) \quad \text{(A-5)}$$

$$\times\, h_p\left(ka\right) P_p^{m-\mu}\left(\cos\theta_{0k}\right) \exp[i\left(m-\mu\right)\phi_{0k}].$$

The Gaunt coefficients $a\left(m, n | -\mu, \nu | p\right)$ and $a\left(m, n | -\mu, \nu | p, p-1\right)$ are expressed in terms of Wigner 3-j symbols $\begin{pmatrix} j_1 & j_2 & j_3 \\ 0 & 0 & 0 \end{pmatrix}$, which are related to Clebsch-Gordon coefficients:

$$a\left(m, n | \mu, \nu | p\right) = (-1)^{m+\mu} (2p+1) \sqrt{\frac{(n+m)!\,(\nu+\mu)!\,(p-m-\mu)!}{(n-m)!\,(\nu-\mu)!\,(p+m+\mu)!}}$$

$$\times \begin{pmatrix} n & \nu & p \\ 0 & 0 & 0 \end{pmatrix} \begin{pmatrix} n & \nu & p \\ m & \mu & -m-\mu \end{pmatrix}, \quad \text{(A-6)}$$

$$a\left(m, n | \mu, \nu | p, q\right) = (-1)^{m+\mu} (2p+1) \sqrt{\frac{(n+m)!\,(\nu+\mu)!\,(p-m-\mu)!}{(n-m)!\,(\nu-\mu)!\,(p+m+\mu)!}}$$

$$\times \begin{pmatrix} n & \nu & q \\ 0 & 0 & 0 \end{pmatrix} \begin{pmatrix} n & \nu & p \\ m & \mu & -m-\mu \end{pmatrix}. \quad \text{(A-7)}$$

The evaluation of the translation coefficients with Stein's formalism leads to a summation on a parameter p by equations (A-4) and (A-5). It seems that since the work by Peterson and Ström,[3] there has been some confusion in the literature about the correct values p takes. Xu recently partially pointed out the problem.[4] Our study leads to the following explanation: Respecting the rules of addition of the kinetic moment, the parameter p should assume all the integer values $p = n \oplus \nu = (n+\nu), (n+\nu-1), (n+\nu-2), ..., |n-\nu|$. However, Wigner 3-$j$ symbols vanish if $j_1+j_2+j_3$ is an odd integer. Then the contribution of the p summation to the $A_{\mu\nu}^{mn}$ coefficient value is null when, due to the Wigner 3-j symbol $\begin{pmatrix} n & \nu & p \\ 0 & 0 & 0 \end{pmatrix}$, p takes the values $(n+\nu-1), (n+\nu-3)$ until $|n-\nu|+1$. In the case of the $B_{\mu\nu}^{mn}$ coefficient, the Wigner 3-j symbol

---

[3]B. Peterson and S. Ström, "T matrix for electromagnetic scattering from an arbitrary number of scatterers and representation of E(3)," *Phys. Rev. D* **8**, 3661–3677 (1973).

[4]Y.-L. Xu, "Electromagnetic scattering by an aggregate of spheres: Far field," *Appl. Opt.* **36**, 9496–9508 (1997).

is $\begin{pmatrix} n & \nu & q \\ 0 & 0 & 0 \end{pmatrix}$, where $q = p - 1$. Then the contribution of the p summation is null when p takes on the following values: $(n + \nu), (n + \nu - 2)$ until $|n - \nu|$. That is, in the evaluation of the $A_{\mu\nu}^{mn}$ coefficients, p takes on the values from $|n - \nu|$ to $(n + \nu)$ in steps of 2; and in the evaluation of the $B_{\mu\nu}^{mn}$ coefficients, p takes on the values from $|n - \nu| + 1$ to $(n + \nu)$ in steps of 2.

The index n is linked to the multipole expansion representative of each dielectric sphere of the cluster. The computation of the T-matrix through the extended boundary condition (EBC) technique requires a truncation of an infinite-dimensional integral matrix equation to a value $n = n_{\max}$. This value must be large enough to correctly represent the physically relevant partial waves, but not too large to be useful numerically. It is usually admitted that Wiscombe's criterion allows an accurate determination of this value.[5] There are as many different $n_{\max}$ as the number of different types and sizes of spheres. We truncate the incident and all the series expansions of the scattered fields at the larger $n_{\max}$ value. Then, f and a are column vectors of dimension $n_{\max} \times 1$.

[5]W. J. Wiscombe, "Improved Mie scattering algorithms," *Appl. Opt.* **19**, 1505–1509 (1980).

Appendix B. Truncation of the Translation Addition Theorem Series

The computation of the N-spheres problem assumes that the series expansions of the translation addition theorem (eq (A-1), (A-2), and (A-3) in app A) are uniformly convergent. Therefore, we can truncate them at $\nu = \nu_{max}$, assuming that the resulting error is small enough if ν_{max} is sufficiently large.

The $\bar{\alpha}(i, j)$ matrices describe the continuity of the tangential components of all the scattered electric fields across each surface of the ith sphere. Then, in an iterative formalism, ν_{max} represents the approximation's order of multiple scattering effects in the system. Its maximal value for convergence is approximately equal to n_{max}. In the recursive algorithm, all multiple-scattering effects are taken into account during the matrix inversion of relation (21) in the main report. Following the analytical coherence of the recursive T-matrix algorithm (RTMA) formalism, $\nu_{max} = n_{max}$. Therefore, $\bar{\alpha}(i, j)$ matrices' dimensions are $[2n_{max}(n_{max} + 2)]^2$.

Relation (17) can also be described as a phase shift of the incident plane wave, when it travels from origins O_o to O_i:

$$\mathbf{a}^i = \mathbf{a}^o \exp\left[ik_{inc} \cdot r_i\right]. \tag{B-1}$$

Starting with $\nu_{max} = n_{max}$, we calculate the absolute variation between the numerical results of equation (B-1) and equation (17) in the main report for each vector's component, due to the variation of ν_{max}. The convergence speed also depends on the distance and orientation between the coordinate systems. Nevertheless, at $\nu_{max} = n_{max}$, the maximal absolute variation is approximately 1. When $\nu_{max} = 2n_{max}$, it is only 6 to 10, and it is not until $\nu_{max} = 3n_{max}$ that an absolute variation of 10 to 15 occurs in the best cases. The dimension of the $\bar{\beta}(i, 0)$ matrices is $4n_{max}(n_{max} + 2) \times \nu_{max}(\nu_{max} + 2)$.

Because of the analytical coherence of the RTMA formalism,[1] the series (eq (A-3)) has to be truncated at the same order ν_{max} as equation (A-2). The dimension of the matrices $\bar{\beta}(0, i)$ is $4\nu_{max}(\nu_{max} + 2) \times n_{max}(n_{max} + 2)$. The limits of convergence that we have encountered for the $\bar{\beta}(i, 0)$ matrices are still present and are propagated into numerical evaluations.

---

[1]W. C. Chew, *Waves and Field in Inhomogeneous Media*, IEEE Press Series on Electromagnetic Waves, 1990.

We can see that if the indices $n_{\max}$ and $\nu_{\max}$ become too large, the numerical evaluations of the matrices $\bar{\alpha}(i,j)$, $\bar{\beta}(i,0)$, and $\bar{\beta}(0,i)$ are limited by the free memory available on the computer, realistic computing time, and numerical convergence of the series. Taking these three factors into account, we see that the computation of the total scattered field by a random cluster in terms of a single expansion on one principal coordinate system is impracticable most of the time. Consequently, the scattering parameter of the sphere cluster (cross sections and scattering matrix) cannot be evaluated.

To circumvent this difficulty, Borghese et al,[2] Mackowski and Mishchenko,[3] and Fuller[4] derived explicit expressions for the total cross sections (scattering, extinction, and absorption) of the sphere cluster, without any need for a single representation of the total scattered field. This formalism is called the sphere-centered formulation. Moreover, Xu[5] recently introduced a formalism to obtain a single expression of the total scattered field in the far-field region. This approach is the most suitable to obtain differential scattering cross sections of an aggregate, without taking the convergence of the translation addition theorem series (eq (A-3)) into account. Indeed, for an arbitrary point M in the far-field region at the vector position $\mathbf{r}$ in the principal system and $\mathbf{r}_i$ in the coordinate system of the ith sphere, one can consider that these two vectors are parallel. By introducing Δ_i as the path variation due to the relative position between the principal and the ith systems, we obtain $r_i = r - \Delta_i$ with $\Delta_i = \mathbf{e}_r \times \mathbf{r}_{0i}$, where $\mathbf{e}_r$ is a unit vector pointed in the direction of M. Then it can be shown that in the far-field region, the translation coefficient can be written as

$$\Re e A^{mn}_{\mu\nu} \left(kr_{0i}, \theta_{0i}, \phi_{0i}\right) = \delta_{n\nu}\delta_{\mu m} \exp\left(-ik\Delta_i\right),$$ (B-2)

$$\Re e B^{mn}_{\mu\nu} \left(kr_{0i}, \theta_{0i}, \phi_{0i}\right) = 0.$$

This formulation leads to a simplification of the analytical formulation of the $\bar{\beta}(0,i)$ matrices. Finally, the total scattered field by the entire cluster of equation (18) can be written in the far-field region as

$$\mathbf{f}^{T(N)} = \sum_{i=1}^{N} \exp\left(-ik\Delta_i\right) \mathbf{f}^{i(N)}.$$ (B-3)

[2]F. Borghese, P. Denti, R. Saija, G. Toscano, and O. I. Sindoni, "Multiple electromagnetic scattering from a cluster of spheres. I. Theory," *Aerosol Sci. Technol.* **3**, 227–235 (1984).

[3]D. W. Mackowski and M. I. Mishchenko, "Calculation of the T matrix and the scattering matrix for ensembles of spheres," *J. Opt. Soc. Am. A* **13**, 2266–2278 (1996).

[4]K. A. Fuller, "Scattering and absorption cross sections of compounded spheres. I. Theory for external aggregation," *J. Opt. Soc. Am. A* **11**, 3251–3260 (1994).

[5]Y.-L. Xu, "Electromagnetic scattering by an aggregate of spheres: Far field," *Appl. Opt.* **36**, 9496–9508 (1997).

Appendix C. Recursive T-Matrix Formulation in the Far-Field Region

Because of the problems introduced in appendices A and B, we introduce a new model of multiple scattering computation by an aggregate of spheres based on the recursive T-matrix algorithm (RTMA) algorithm developed by Chew,[1] modified to bypass the convergence problem of equation (A-1) in appendix A. Indeed, the evaluation of the incident field on each sphere is made through a phase shift formalism instead of a matrix calculation. Then, in the second stage, to circumvent the convergence problem of equation (A-3), we use the far-field approximation introduced by Xu.[2] The fundamental equations of this model are

$$\bar{\mathbf{T}}^{N+1(N+1)} = \left[\bar{\mathbf{I}} - \bar{\mathbf{T}}^{N+1(1)} \sum_{i=1}^{n} \bar{\alpha}(N+1, i) \bar{\mathbf{T}}^{i(N)} \bar{\alpha}(i, N+1)\right]^{-1} \tag{C-1}$$

$$\times \ \bar{\mathbf{T}}^{N+1(1)} \left[\bar{\mathbf{I}} + \sum_{i=1}^{n} \bar{\alpha}(N+1, i) \bar{\mathbf{T}}^{i(N)} \exp\left[\mathrm{i}\mathbf{k}_{\mathrm{inc}}\left(\mathbf{r}_{N+1} - \mathbf{r}_i\right)\right]\right],$$

$$\bar{\mathbf{T}}^{i(N+1)} = \bar{\mathbf{T}}^{i(N)} \left[\bar{\mathbf{I}} + \bar{\alpha}(i, N+1) \bar{\mathbf{T}}^{N+1(N+1)} \exp\left[\mathrm{i}\mathbf{k}_{\mathrm{inc}}\left(\mathbf{r}_{N+1} - \mathbf{r}_i\right)\right]\right], \ i \leq N, \tag{C-2}$$

$$\mathbf{f}^{(N+1)} = \sum_{i=1}^{N+1} \mathbf{f}^{i(N+1)} \exp\left(-\mathrm{i}k\Delta_i\right), \tag{C-3}$$

$$\mathbf{f}^{i(N+1)} = \bar{\mathbf{T}}^{i(N+1)} \mathbf{a}^0 \exp\left(\mathrm{i}\mathbf{k}_{\mathrm{inc}} \times \mathbf{r}_i\right). \tag{C-4}$$

---

[1]W. C. Chew, *Waves and Field in Inhomogeneous Media*, IEEE Press Series on Electromagnetic Waves, 1990.

[2]Y.-L. Xu, "Electromagnetic scattering by an aggregate of spheres: Far field," *Appl. Opt.* **36**, 9496–9508 (1997).

Distribution

Admnstr
Defns Techl Info Ctr
Attn DTIC-OCP
8725 John J Kingman Rd Ste 0944
FT Belvoir VA 22060-6218

Central Intllgnc Agency Dir DB Standard
Attn OSS/KPG/DHRT
1E61 OHB
Washington DC 20505

Dir of Defns Rsrch & Engrg
Attn DD TWP
Attn Engrg
Washington DC 20301

Ofc of the Secy of Defns
Attn ODDRE (R&AT)
The Pentagon
Washington DC 20301-3080

Ofc of the Secy of Defns
Attn OUSD(A&T)/ODDR&E(R) R J Trew
3080 Defense Pentagon
Washington DC 20301-7100

Commanding Officer
Attn NMCB23
6205 Stuart Rd Ste 101
FT Belvoir VA 22060-5275

AMCOM MRDEC
Attn AMSMI-RD W C McCorkle
Redstone Arsenal AL 35898-5240

CECOM
Attn PM GPS COL S Young
FT Monmouth NJ 07703

Dir for MANPRINT
Ofc of the Deputy Chief of Staff for Prsnnl
Attn J Hiller
The Pentagon Rm 2C733
Washington DC 20301-0300

Dir of Chem & Nuc Ops DA DCSOPS
Attn Techl Lib
Washington DC 20301

US Army ARDEC
Attn AMSTA-AR-TD M Fisette
Bldg 1
Picatinny Arsenal NJ 07806-5000

US Army Engrg Div
Attn HNDED FD
PO Box 1500
Huntsville AL 35807

US Army Info Sys Engrg Cmnd
Attn ASQB-OTD F Jenia
FT Huachuca AZ 85613-5300

US Army Natick RDEC Acting Techl Dir
Attn SSCNC-T P Brandler
Natick MA 01760-5002

US Army NGIC
Attn Rsrch & Data Branch
220 7th Stret NE
Charlottesville VA 22901-5396

US Army Nuc & Cheml Agency
7150 Heller Loop Ste 101
Springfield VA 22150-3198

US Army Simulation, Train, & Instrmntn
  Cmnd
Attn J Stahl
12350 Research Parkway
Orlando FL 32826-3726

US Army Strtgc Defns Cmnd
Attn CSSD H MPL Techl Lib
PO Box 1500
Huntsville AL 35807

US Army Tank-Automtv Cmnd Rsrch, Dev, &
  Engrg Ctr
Attn AMSTA-TR J Chapin
Warren MI 48397-5000

US Army Train & Doctrine Cmnd Battle Lab
  Integration & Techl Dirctrt
Attn ATCD-B J A Klevecz
FT Monroe VA 23651-5850

TECOM
Attn AMSTE-CL
Aberdeen Proving Ground MD 21005-5057

US Army Soldier & Biol Chem Cmnd Dir of
  Rsrch & Techlgy Dirctrt
Attn SMCCR-RS I G Resnick
Aberdeen Proving Ground MD 21010-5423

US Military Academy
Mathematical Sci Ctr of Excellence
Attn MDN-A LTC M D Phillips
Dept of Mathematical Sci Thayer Hall
West Point NY 10996-1786

Chief of Nav OPS Dept of the Navy
Attn OP 03EG
Washington DC 20350

Nav Surface Warfare Ctr
Attn Code B07 J Pennella
17320 Dahlgren Rd Bldg 1470 Rm 1101
Dahlgren VA 22448-5100

DARPA
Attn S Welby
Attn Techl Lib
3701 N Fairfax Dr
Arlington VA 22203-1714

US Dept of Energy
Attn KK 22 K Sisson
Attn Techl Lib
Washington DC 20585

Hicks & Associates Inc
Attn G Singley III
1710 Goodrich Dr Ste 1300
McLean VA 22102

Director
US Army Rsrch Ofc
Attm AMSRL-RO
Attn AMSRL-RO-EN W Bach
PO Box 12211
Research Triangle Park NC 27709

US Army Rsrch Lab
Attn AMSRL-DD J M Miller
Attn AMSRL-CI-AI-A Mail & Records Mgmt
Attn AMSRL-CI-AP Techl Pub (3 copies)
Attn AMSRL-CI-LL Techl Lib (3 copies)
Attn AMSRL-IS-EE G Videen (5 copies)
Adelphi MD 20783-1197

REPORT DOCUMENTATION PAGE

Form Approved
OMB No. 0704-0188

1. AGENCY USE ONLY *(Leave blank)*	2. REPORT DATE March 2000	3. REPORT TYPE AND DATES COVERED Final, Dec 98 to Jan 99

4. TITLE AND SUBTITLE Observations and Calculations of Light Scattering from Clusters of Spheres

5. FUNDING NUMBERS

DA PR: B53A

PE: 61102A

6. AUTHOR(S) Stephen Holler (Yale University), Jean-Claude Auger, Brian Stout (Université Pierre et Marie Curie), Yongle Pan (New Mexico State University), Jerold R. Bottiger (U.S. Army Edgewood Chemical Biological Center), Richard K. Chang (Yale University), Gorden Videen (ARL)

7. PERFORMING ORGANIZATION NAME(S) AND ADDRESS(ES)
U.S. Army Research Laboratory
Attn: AMSRL-IS-EM   email: gvideen@arl.mil
2800 Powder Mill Road
Adelphi, MD 20783-1197

8. PERFORMING ORGANIZATION REPORT NUMBER
ARL-TR-2136

9. SPONSORING/MONITORING AGENCY NAME(S) AND ADDRESS(ES)
U.S. Army Research Laboratory
2800 Powder Mill Road
Adelphi, MD 20783-1197

10. SPONSORING/MONITORING AGENCY REPORT NUMBER

11. SUPPLEMENTARY NOTES
ARL PR: 7FEJ70
AMS code: 61110253A11

12a. DISTRIBUTION/AVAILABILITY STATEMENT Approved for public release; distribution unlimited.

12b. DISTRIBUTION CODE

13. ABSTRACT *(Maximum 200 words)*
Two-dimensional angular optical scattering (TAOS) from clusters of polystyrene latex spheres is measured in the near-forward and near-backward directions. In both cases, the scattering pattern contains a rich and complicated structure due to the interaction and interference of the light among the primary particles. Calculations are made for aggregates similar to those generated experimentally that demonstrate the rich structure in the scattering pattern. A comparison of the experimental and theoretical TAOS gives good qualitative agreement.

14. SUBJECT TERMS TAOS, aggregates, particles, biowarfare	15. NUMBER OF PAGES 39
	16. PRICE CODE

17. SECURITY CLASSIFICATION OF REPORT Unclassified	18. SECURITY CLASSIFICATION OF THIS PAGE Unclassified	19. SECURITY CLASSIFICATION OF ABSTRACT Unclassified	20. LIMITATION OF ABSTRACT UL